P1.1 TOP-OF-ATMOSPHERE DIRECT RADIATIVE EFFECT OF AEROSOLS FROM THE CLOUDS AND THE EARTH'S RADIANT ENERGY SYSTEM (CERES) SATELLITE INSTRUMENT OVER THE TROPICAL OCEANS

N. G. Loeb* and S. Kato
Hampton University, Hampton, VA

1. INTRODUCTION

Recent studies have demonstrated the potential influence of aerosols on top-of-atmosphere (TOA) and surface radiation budgets. Aerosols affect the radiation budget directly by scattering and absorbing solar and thermal infrared radiation, and indirectly by modifying the microphysical and radiative properties of clouds. The present study focuses on the TOA direct radiative effect of aerosols over ocean derived from the Clouds and the Earth's Radiant Energy System (CERES) instrument onboard the Tropical Rainfall Measuring Mission (TRMM) spacecraft.

2. OBSERVATIONS

CERES/TRMM was launched on November 27, 1997, as part of the Tropical Rainfall Measuring Mission (TRMM). In this study, nine available months of the CERES/TRMM Single Scanner Footprint TOA/Surface Fluxes and Clouds (SSF) product from January-August 1998, and March 2000, between 35°S and 35°N are considered. The CERES SSF product combines CERES measurements of reflected shortwave (SW), emitted longwave (LW) and emitted window (WN) radiances and fluxes with coincident Visible Infrared Scanner (VIRS) retrievals of aerosol and cloud properties. VIRS aerosol and cloud properties are convolved over the CERES footprint with the CERES point spread function. Also included in this product are meteorological fields based on European Centre for Medium-Range Weather Forecasts (ECMWF) data assimilation analysis (Rabier et al, 1998). The CERES instrument has a resolution at nadir of approximately 10 km (equivalent diameter) and operates in three scan modes: cross-track, along-track, and rotating azimuth plane (RAP) mode, where the instrument scans in elevation as it rotates in azimuth. The VIRS instrument is a five-channel imaging spectroradiometer that measures radiation at 0.63 μm, 1.61 μm, 3.78 μm, 10.8 μm and 12.0 μm. VIRS is similar to the AVHRR instrument but has a 2.11-km resolution at nadir compared to 1.1 km for AVHRR.

*Corresponding author address: Norman G. Loeb, Mail Stop 420, NASA Langley Research Center, Hampton, VA 23681-2199; e-mail: n.g.loeb@larc.nasa.gov

3. METHODOLOGY

The top-of-atmosphere direct radiative effect of aerosols for a given location at latitude λ and longitude ψ on a given day (d) is defined as follows:

$$\Delta F(\lambda,\psi,d) = \bar{F}_{na}(\lambda,\psi,d) - \bar{F}_{a}(\lambda,\psi,d) \qquad (1)$$

where $\bar{F}_{na}(\lambda,\psi,d)$ is the daily average SW flux in the absence of aerosols, and $\bar{F}_{a}(\lambda,\psi,d)$ is the daily average SW flux in the presence of aerosols. $\Delta F(\lambda,\psi,d)$ is determined from instantaneous CERES TOA fluxes that are converted to daily averages over 1°x1° regions. To avoid problems with specular reflection from the ocean surface, the analysis is restricted to solar zenith angles less than 60°, viewing zenith angles less than 70°, and glint angles (angle between reflected ray and specular ray for a flat ocean) greater than 40°.

Daily average fluxes in the presence of aerosols ($\bar{F}_{a}(\lambda,\psi,d)$) are inferred from instantaneous fluxes estimated from CERES broadband unfiltered radiances. The radiances are converted to flux using empirical Angular Distribution Models (ADMs) (Loeb et al., 2002). Each instantaneous flux is converted to a daily average by estimating what the corresponding flux would be under the same conditions at all other times of the day. To estimate the flux at any given time, directional models of normalized TOA albedo as a function of solar zenith angle are applied. The directional models are derived from the empirical Angular Distribution Models (ADMs).

The daily average flux in the absence of aerosols ($\bar{F}_{na}(\lambda,\psi,d)$) is inferred from a simple regression procedure. Instantaneous TOA fluxes from CERES are plotted against VIRS 0.63 μm aerosol optical depths in 1° solar zenith angle increments. VIRS 0.63 μm aerosol optical depths are retrieved using the 2nd generation NOAA/NESDIS algorithm (Stowe et al., 1997), which has been implemented in the CERES SSF production code. The intercept for these regressions—i.e. the TOA flux extrapolated to zero aerosol optical depth—approximates the "no aerosol flux" ($F_{na}(\theta_o)$) in each 1° solar zenith angle increment. Comparisons between empirical and theoretical $F_{na}(\theta_o)$ are provided in Kato and Loeb (2002).

Clear ocean scenes are identified using a cloud mask (Trepte et al., 1999) applied to the VIRS pixel data. The CERES cloud mask uses data from 5 VIRS channels to determine whether individual pixels contain cloud, glint, smoke or fire signatures.

To examine the sensitivity to cloud contamination, two threshold tests are considered in addition to those described in Trepte et al. (1999). The first is a spatial homogeneity test applied to VIRS pixels: if the maximum and minimum 0.63 μm reflectance from a 2 x 2 VIRS pixel array differs by more than a threshold value of 0.003, the pixels are considered potentially cloud contaminated. A second test identifies pixels with a 3.78 μm channel reflectance >0.03 as also potentially cloud contaminated. Thresholds for these tests are selected based on the analysis of Stowe et al. (1999).

If all VIRS pixels within a CERES footprint pass the reflectance, brightness temperature, and infrared/near infrared difference tests, and more than 50% pass the spatial homogeneity and 3.78 μm channel reflectance tests, these footprints are considered clear and are included in the analysis.

4. RESULTS

Fig. 1 shows the latitudinal distribution of the direct radiative effect of aerosols and VIRS 0.63 μm aerosol optical depth. In both cases, a marked contrast between the northern and southern tropical oceans is evident. The direct radiative effect in the south is –3.6 W m^{-2} compared to -5.5 W m^{-2} in the north. The corresponding VIRS 0.63 μm aerosol optical depths are 0.11 and 0.17, respectively. Over all the tropics, the average direct radiative effect is –4.6 W m^{-2} and the average VIRS 0.63 μm aerosol optical depth is 0.14.

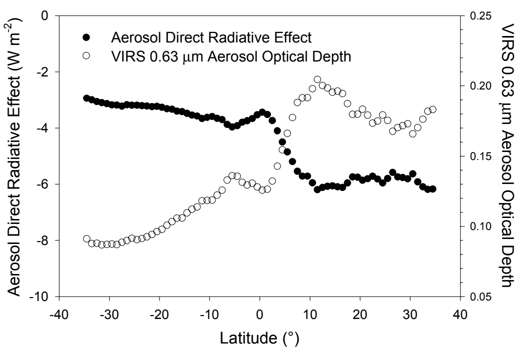

Figure 1 Latitudinal distribution of the direct radiative effect of aerosols and VIRS 0.63 μm aerosol optical depth.

Fig. 2 (a) shows the solar zenith angle dependence in the derivative of aerosol direct radiative effect (in terms of albedo) with VIRS 0.63 μm aerosol optical depth ($\Delta\alpha/\Delta\tau$) over the Kaashidoo Climate Observatory (KCO) between January-April, 1998, and May-August, 1998. The January-April period over KCO is associated with highly polluted air from the Indian subcontinent (Satheesh and Ramanathan, 2000), whereas cleaner conditions prevail during the May-August period due to increased precipitation and a shift in wind direction from northeasterly to southerly. Fig. 2 (a) shows smaller $\Delta\alpha/\Delta\tau$ during the polluted January-April period compared to the cleaner May-August period. This is consistent with what is expected theoretically: smaller $\Delta\alpha/\Delta\tau$ is associated with larger particles and/or increased particle absorption; larger $\Delta\alpha/\Delta\tau$ occurs when particles are small and/or less absorbing. As expected, the "no aerosol" condition—represented by the intercept in Fig. 2 (b)—shows little or no difference for these two time periods. East of the Indian subcontinent (for 0°-20°N, 60°E-80°E), the daily average flux per unit VIRS 0.63 μm aerosol optical depth for these two periods is -26.8 W m^{-2} τ^{-1} for January-April, 1998 (consistent with Satheesh and Ramanathan, 2000), and -29.4 W m^{-2} τ^{-1} for May-August, 1998.

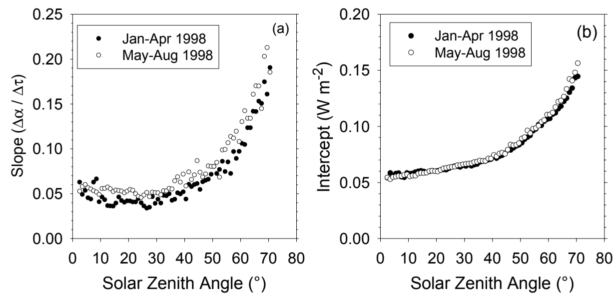

Figure 2 (a) Slope and (b) intercept of CERES albedo against VIRS aerosol optical depth as function of solar zenith angle over the Kaashidoo Climate Observatory (KCO) between January-April, 1998, and May-August, 1998.

To examine the influence of biomass burning aerosols on TOA radiation during a dramatic fire event, we consider the 1998 Central American fires that occurred during a period of prolonged drought over Central America and southern Mexico (Peppler et al., 2000). Fig. 3 shows the spatial and temporal variation of the aerosol direct radiative effect and the corresponding VIRS 0.63 μm aerosol optical depth for three longitude intervals off of the coast of Mexico. The region furthest from the source of the biomass burning, between 140°W-120°W, has a minimum direct radiative effect of –2.4 W m^{-2} (aerosol optical depth of 0.08) in January, and a maximum in June of –5 W m^{-2} (aerosol optical depth of 0.14). Between 120°W-100°W, the radiative effect ranges from –2.5 W m^{-2} (aerosol optical depth of 0.09) in January to –18 W m^{-2} (aerosol optical depth of 0.58) in May. Closest to the source region, between 100°W-90°W, a minimum of –4.7 W m^{-2} (aerosol optical depth of 0.17) occurs in January—likely due to urban pollution in Mexico City—to a maximum of –32.5 W m^{-2} (aerosol optical depth 0.96) in May due to biomass burning. These results are consistent with Christopher et al. (2000) who found instantaneous SW forcing over the same region and period of ≈-68 W m^{-2}, which correspond roughly to a daily mean of -34 W m^{-2}.

When the direct radiative effect of aerosols is stratified by wind speed, a small yet systematic trend is observed. Fig. 4 shows the direct radiative effect against wind speed for regions with mean VIRS 0.63 μm aerosol optical depths < 0.25 for 15°N - 25°N and 90°W to 180°W. As shown, the direct radiative effect becomes more pronounced over this region as wind speeds become stronger. This trend may be physical, as one might expect more sea-salt aerosol generation with increasing wind speed, or it could be due to increased transport of aerosols from source regions.

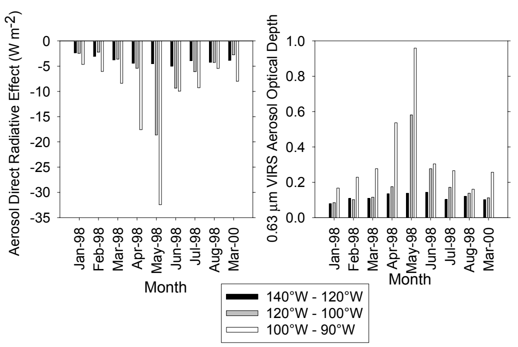

Figure 3 Spatial and temporal variation of (a) the direct radiative effect and (b) VIRS 0.63 m aerosol optical depth for biomass burning aerosols near Mexico for latitudes between 15 N - 25 N and the indicated longitudes.

Alternately, this trend may instead be an artifact of the retrieval. For example, at large wind speeds, whitecap coverage may increase the observed reflectance from the surface, which can be misinterpreted as an increase in the aerosol direct effect. Haywood et al. (1999) found a similar trend in their comparison of the direct radiative effect of aerosols based on ERBE measurements. In that case, regions where the direct radiative effect was a maximum coincided with regions where the wind speed was a maximum.

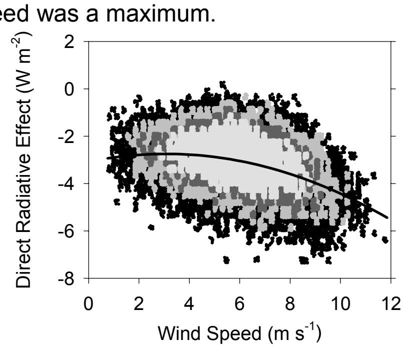

Figure 4 Aerosol direct radiative effect against wind speed for 1° regions with mean VIRS 0.63 μm aerosol optical depths < 0.25 for 15°N - 25°N and 90°W to 180°W. Solid line is a linear regression 2nd order polynomial fit through all data points.

One of the largest uncertainties in estimating the direct radiative effect of aerosols from satellite measurements is cloud contamination. As noted in earlier, the cloud mask involves several threshold tests to identify cloud-free CERES footprints. In the present study, footprints are assumed to be cloud-free if all VIRS pixels within a CERES footprint pass the reflectance, brightness temperature, and infrared/near infrared difference tests, and more than 50% pass the spatial homogeneity and 3.78 μm channel reflectance tests. The direct effect was also determined using thresholds of 0% and 100% for the percentage of VIRS pixels within a CERES footprint that pass the spatial homogeneity and 3.78 μm channel reflectance tests. The 0% threshold includes all footprints that pass the reflectance, brightness temperature, and infrared/near infrared difference tests, while the 100% threshold requires all pixels within a footprint to also pass the spatial homogeneity and 3.78 μm channel reflectance tests. Fig. 5 compares the latitudinal dependence in the direct effect for a 50% threshold (solid circles) with results based on thresholds of 0% (bottom gray line) and 100% (top gray line). On average, the difference between the two extreme cases (i.e. 0% and 100%) is $\approx$0.8 W m^{-2}. The direct effect based on the 50% threshold is closer to the 100% threshold result ($\approx$0.29 W m^{-2}) than it is to the 0% threshold values ($\approx$0.46 W m^{-2}). Unfortunately, it remains unclear how this error would change with higher-resolution imager measurements (e.g. 0.25 km MODIS measurements). The higher-resolution data would likely significantly improve detection of small-scale and thin clouds, which would tend to reduce the magnitude of the direct effect. However, there may also be conditions in which the current cloud mask is too restrictive and misidentify thicker aerosol layers for cloud. Clearly, more study is needed using instruments that are more sensitive to the presence of cloud (e.g. MODIS, CALIPSO).

For comparison, Fig. 5 also shows how the direct effect changes when the imager scene identification is replaced by scene identification from the CERES/TRMM "ERBE-Like" product (open circles), and when both the ERBE-like ADMs and scene identification are used to determine the direct effect (solid triangles). The ERBE-like product uses the Maximum Likelihood Estimation Technique (MLE) (Wielicki and Green, 1989) applied to CERES broadband radiances in order to classify a footprint as either clear, partly cloudy, mostly cloud or overcast. ERBE ADMs were derived from Nimbus-7 Earth Radiation Budget (ERB) measurements.

When ERBE-like clear ocean scene identification is used in conjunction with ADMs constructed from the SSF (open circles), the average direct effect reaches $\approx$-9 W m^{-2}, a change of $\approx$-4.4 W m^{-2} (or a factor of 2) over what is obtained when the imager is used for scene identification. When ERBE-like ADMs are used with MLE scene identification (solid triangles), the average direct effect reaches -7.5 W m^{-2}, or $\approx$-3 W m^{-2} more than the SSF value. Clearly, this extra "forcing" is caused by cloud contamination. For ERBE, the cloud contamination problem is even more pronounced because the ERBE scanner footprint is at least 4 times larger than a CERES/TRMM footprint. Loeb et al. (2001) showed that an increase in footprint size by a factor of 4 causes a 6% increase in clear-sky ocean radiance using the MLE technique. This occurs because there is a greater likelihood of encountering undetected sub-resolution cloud when the footprint size is large. Assuming a daily average clear ocean SW flux of 40 W m^{-2}, a 6% increase in SW flux due to cloud contamination would increase the ERBS SW flux by 2.4 W m^{-2} above the CERES ERBE-like SW flux. This means the direct effect for ERBE/ERBS would reach –10 W m^{-2}, or $\approx$-5.4 W m^{-2} above the SSF value.

Other factors influencing the uncertainty in the direct effect are instrument calibration and the conversion of filtered SW radiance to unfiltered SW radiance. For CERES/TRMM, the absolute uncertainty in the SW radiances is $\approx$1% (Priestley et al., 2000), which corresponds to a 0.4 W m^{-2} uncertainty in clear-sky TOA

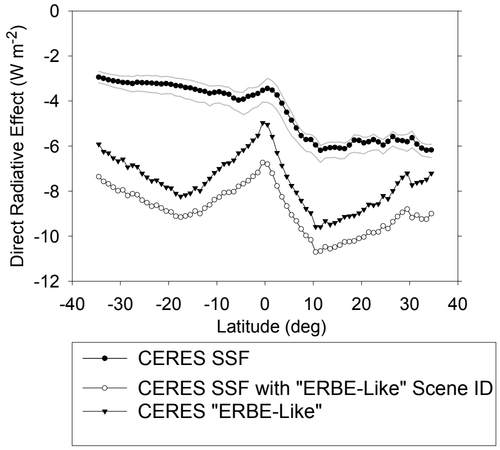

Figure 5 Sensitivity of aerosol direct radiative effect to clear-sky scene identification.

flux, assuming a daily average clear-sky flux of 40 W m^{-2}. The uncertainty in the conversion of filtered SW radiance to unfiltered SW radiance is ≈1% (Loeb et al., 2001). Assuming the error due to cloud contamination is 0.8 W m^{-2} (corresponding to the difference in flux between the upper and lower gray lines in Fig. 5 that bound the "CERES SSF" aerosol direct radiative effect estimate), and combining errors from cloud contamination, radiance-to-flux conversion, radiance unfiltering and calibration, the overall error becomes $(0.8^2+0.2^2+0.4^2+0.4^2)^{1/2}$ W m-2 or ≈1 W m-2 (≈20%). Because of increased cloud contamination associated with the MLE technique, the uncertainty in the CERES ERBE-like direct effect is approximately 3 W m^{-2}. As noted earlier, the cloud contamination problem for ERBE/ERBS is even worse due to its larger footprint. In that case, the error in the direct effect likely reaches 5.5 W m^{-2}.

5. SUMMARY

This study demonstrates how broadband fluxes from CERES combined with high-resolution imager measurements can be used to estimate the direct radiative effect of aerosols over ocean. Based on 9 months of CERES/TRMM measurements, the average direct effect over the tropical oceans is estimated to be -4.6 W m^{-2}. Over the southern tropical oceans, the magnitude of the direct effect is ≈2 W m^{-2} smaller than over the northern tropical oceans.

While the measurements considered in this study cannot be used to provide accurate estimates of the anthropogenic component of the aerosol direct effect over the tropics, the combination of CERES/Aqua, MODIS/Aqua and CALIPSO measurements will significantly improve our ability to do so. With these measurements, the anthropogenic aerosol direct effect can be estimated from CERES fluxes over regions identified as having a significant anthropogenic component according to transport model back trajectory analyses initialized using vertical layer information from CALIPSO measurements and particle size and optical depth information from MODIS. Furthermore, the higher spatial resolution of MODIS data combined with CALIPSO's improved ability to distinguish cloud from aerosol layers will reduce errors due to cloud contamination.

6. REFERENCES

Christopher, S.A., et al., 2000: Shortwave direct radiative forcing of biomass burning aerosols estimated from VIRS and CERES. Geophys. Res. Letters, 27, 2197-2200.

Haywood, J.M., V. Ramaswamy, and B.J. Soden, 1999: Tropospheric aerosol climate forcing in clear-sky satellite observations over the oceans. Science, 283, 1299-1303.

Kato, S., et al., 2002: Estimate of top-of-atmosphere albedo for a molecular atmosphere over ocean using CERES measurements, J. Geophys. Res. (accepted).

Loeb, N.G., et al., 2001: Determination of unfiltered radiances from the CERES instrument. J. Appl. Meteor., 40, 822-835.

Loeb, N.G., et al., 2002: Angular distribution models for top-of-atmosphere radiative flux estimation from the CERES Instrument on the Tropical Rainfall Measuring Mission Satellite. Part I: Methodology, *J. Appl. Meteor.*, submitted, 2002.

Peppler, R.A., et al., 2000: ARM Southern Great Plains site observations of the smoke pall associated with the 1998 Central American fires. Bull. Amer. Meteor., 81, 2563-2591.

Priestley, K.J., et al., 2000: Post launch radiometric validation of the CERES proto-flight model on the Tropical Rainfall Measuring Mission (TRMM) spacecraft through 1999. J. Appl. Meteor., 39, 2249-2258.

Rabier, F., J.-N. Thepaut, and P. Courtier, 1998: Extended assimilation and forecast experiments with a four-dimensional variational assimilation, *Quart. J. Roy. Meteor. Soc.*, **124**, 1861-1887.

Satheesh, S.K., and V. Ramanathan, 2000: Large differences in tropical aerosol forcing at the top the atmosphere and Earth's surface. Nature, 405, 60-63.

Stowe, L.L., P.A. Davis, and E.P. McClain, 1999: Scientific basis and initial evaluation of the CLAVR-1 global clear/cloud classification algorithm for the Advanced Very High Resolution Radiometer. J. Atmos. Oceanic Tech., 16, 656-681.

Stowe, L.L., A.M. Ignatov, and R.R. Singh, 1997: Development, validation and potential enhancements to the second generation operational aerosol product at NOAA/NESDIS, J. Geophys. Res., 102, 16,923 – 16,934.

Trepte, Q., Y. Chen, S. Sun-Mack, P. Minnis, D. F. Young, B. A. Baum, and P. W. Heck, 1999: Scene identification for the CERES cloud analysis subsystem. Preprints, *10th Conf. on Atmospheric Radiation,* Madison, WI, Amer. Meteor. Soc., 169–172. *Amer. Meteor. Soc.,* **77,** 853–868.

Wielicki, B.A., and R.N. Green, 1989: Cloud identification for ERBE radiation flux retrieval. J. Appl. Meteor., 28, 1133-1146.